NASA

Technical Memorandum 80590

Characteristics of the Telescope for High Energy γ-Ray Astronomy Selected for Definition Studies on the Gamma Ray Observatory

E.B. Hughes, R. Hofstadter, A. Johansson, J. Rolfe, D.L. Bertsch, W.J. Cruickshank, C.H. Ehrmann, C.E. Fichtel, R.C. Hartman, D.A. Kniffen, R.W. Ross, D.J. Thompson, K. Pinkau, H. Rothermel, M. Sommer, H. Mayer-Hasselwander, A. Favale and E. Schneid

OCTOBER 1979

National Aeronautics and Space Administration

Goddard Space Flight Center
Greenbelt, Maryland 20771

SUMMARY

The high energy γ-ray telescope selected for definition studies on the Gamma Ray Observatory provides a substantial improvement in observational capability over earlier instruments. It will have about 20 times more sensitivity, cover a much broader energy range, have considerably better energy resolution and provide a significantly improved angular resolution. The design and performance are described.

Presented at the

IEEE 1979 Nuclear Science Symposium
Oct. 17-19, 1979, San Francisco, Ca.

OCTOBER 1979

CHARACTERISTICS OF THE TELESCOPE FOR HIGH ENERGY γ-RAY ASTRONOMY SELECTED FOR DEFINITION STUDIES ON THE GAMMA RAY OBSERVATORY

E.B. Hughes, R. Hofstadter, A. Johansson* and J. Rolfe

High Energy Physics Laboratory and Department of Physics†
Stanford University
Stanford, California 94305

D.L. Bertsch, W.J. Cruickshank, C.H. Ehrmann, C.E. Fichtel,
R.C. Hartman, D.A. Kniffen, R.W. Ross and D.J. Thompson

NASA Goddard Space Flight Center
Greenbelt, Maryland 20771

K. Pinkau, H. Rothermel, M. Sommer and H. Mayer-Hasselwander

Max-Planck-Institut für Extraterrestrische Physik
8046 Garching b.
München, Germany

A. Favale and E. Schneid

Grumman Aerospace Corporation
Bethpage, L.I., New York 11714

†Work supported by the National Aeronautics and Space Administration under Grants NAS5-25544 and NGR05-020-452.

*Permanent address: The Tandem Accelerator Laboratory, Box 533,
S 751 21 Uppsala, Sweden.

I. INTRODUCTION

The high energy γ-ray telescope to be described in this paper is one of five instruments selected for definition studies on the Gamma Ray Observatory mission (GRO) which is currently being considered by NASA for launch in the mid 1980's. GRO is intended to explore the γ-ray window to the universe from 0.1 MeV to over 10^4 MeV. The high energy γ-ray telescope on GRO will cover the energy range from about 20 MeV to 2×10^4 MeV with more than an order of magnitude greater sensitivity than the earlier high energy γ-ray instruments carried on SAS-2 and COS-B. It will also have better angular and energy resolution and a wider dynamic range of accepted energies than these earlier instruments.

The SAS-2 and COS-B satellites have already demonstrated that high energy γ-ray astronomy can make major contributions to astrophysics, especially in areas involving very high energy processes. Gamma-ray emission has been detected from the galactic plane, the spiral arms, pulsars and extragalactic objects, as well as sources not yet identified at other wavelengths. A diffuse radiation, presumably extragalactic, has also been observed. The high energy γ-ray telescope on GRO should provide the opportunity to move from the recent discovery phase of high energy γ-ray astronomy to an exploratory and definition phase.

II. INSTRUMENT DESIGN

A. Design Requirements

The instrument must have the ability to detect and to identify incident γ-rays clearly. Since the detection is by means of the unique signature of the pair production process, it is important not only that the vertex of the electron pair be seen, but also that enough track length of the secondary electrons be observed to reveal their separation. Further, an unambiguous picture

must be obtained wherein secondary and other tracks are visible. The relatively high fluxes of cosmic rays, Earth albedo and trapped radiation require that these radiations and their secondaries be rejected very efficiently. This elimination process must be one that neither significantly reduces the live-time of the instrument, nor uses an intolerable portion of the data bits available for the γ-ray information. A high sensitivity is required, dictating a large area, as large a conversion efficiency as possible consistent with other requirements, and as wide an acceptance angle as possible while avoiding the Earth albedo γ-rays and secondaries from surrounding materials. Good determination of the γ-ray arrival direction is required for the observation of localized objects and the detailed study of galactic structure. A wide dynamic range and good resolution in the measurement of γ-ray energies are required for the understanding of the emission mechanisms. Precise timing of the detected γ-rays is required for the study of variable pulsed emission from fast pulsars. The complete instrument must be compatible with the Shuttle launch environment and extended operation in space.

B. Principles of Operation

The operating principle of the instrument is illustrated in the simplified schematic of Fig. 1. A γ-ray entering from the top may convert to an electron-positron pair by interacting in one of the thin tantalum sheets interleaved between the closely-spaced spark chamber modules. The secondary electron-positron pair then intercepts an upper array of plastic scintillation trigger counters, passes through a set of widely-spaced spark chamber modules, intercepts a lower array of trigger counters and finally enters a NaI(Tl) crystal spectrometer, where its energy is dissipated in an electromagnetic cascade. If the large plastic anticoincidence shield has not been triggered and if signals are received from the upper and lower counter arrays

with a downward-moving time-of-flight signature, then a high voltage pulse is applied to the spark chamber modules, and subsequently the event data is recorded. Events are accepted even if one of the secondary particles is scattered in the upper spark chamber modules and does not intercept the lower trigger counters or the NaI(Tℓ) crystal. For such events, the energy of the escaping particle may be estimated from the degree of multiple scattering observed. The appearance of the characteristic electron-positron pair in the spark chamber confirms the detection of a γ-ray and an analysis of the tracks reveals the γ-ray direction from an appropriately weighted average of the electron and positron directions. The NaI(Tℓ) crystal provides the γ-ray energy and the event time is given by an on-board clock.

C. Coincidence and Time-of-Flight System

The trigger counters and the coincidence system, which include the directional time-of-flight circuitry, are used to trigger the spark chamber and initiate analysis and data read-out when an acceptable event occurs. The counter telescope consists of two 4 x 4 arrays of square plastic scintillator tiles, each coupled by an adiabatic light guide to a fast photomultiplier tube. Each tile array is 81 cm x 81 cm and the two arrays are separated by 60 cm. Of the 256 possible combinations of one upper tile and one lower tile, 96 are selected by the coincidence logic. The other combinations have highly oblique viewing directions and could possibly be triggered by secondary particles from interactions in materials outside the field-of-view. Each of the 96 acceptable two-fold coincidences contributes to one of nine acceptable viewing directions within the total angular aperture. It is therefore possible to turn off each direction mode when it begins to see albedo γ-rays from the Earth's horizon, without necessarily deactivating that part of the aperture that is still looking into space. The direction modes are controlled independently by commands to the

coincidence system, either sent from the ground or generated automatically on the spacecraft.

In addition to defining the aperture of the instrument, the two arrays of scintillator tiles also determine, by a time-of-flight measurement, whether a particle is traversing the detector in a downward or upward direction. To permit the immediate rejection of upward-moving particles, the time-of-flight analysis must be completed before the trigger pulse is delivered to the high voltage pulser. Since the spark chamber must be pulsed within about 500 nsec after the passage of the γ-ray through the instrument, the time-of-flight analysis must be completed within about 400 nsecs. An electronic system with this capability, but for a different tile geometry, is described in an accompanying article by Ross and Chesney[1].

The electronic signature required to generate a master event trigger (MET) requires (a) a two-fold coincidence in one or more of the 96 acceptable tile combinations, (b) the enablement of the corresponding direction mode, (c) the absence of a veto signal in the anticoincidence system, (d) an acceptable time-of-flight, and (e) the completed read-out of the preceeding event. The MET initiates the pulsing of the spark chambers and their subsequent read-out, the digitization and read-out of the signal from the NaI(Tℓ) crystal, and the recording of other event data.

D. Anticoincidence System

The function of the large anticoincidence scintillator is to reject charged particles with very high efficiency. This detector is designed so that its inefficiency is less than 10^{-6}. Both calculations and laboratory tests show that this requirement can be met with the scintillator to be used on the GRO instrument[2]. The required dome will be formed from a single piece of plastic scintillator 2 cm in thickness and will be viewed by an array of twenty-four 3.5 cm photomultiplier tubes around its lower edge.

Each of the phototubes viewing the anticoincidence dome contains its own high-voltage supply and preamplifier. Signals from groups of six preamplifiers are linearly combined and separately discriminated. For reliability, the four resultant signals are combined by two AC-coupled OR gates to produce two independent veto signals. These signals are stretched if a second charged particle is detected within the original veto interval.

The anticoincidence dome will be mounted as a free-standing shell above the spark chamber pressure vessel (see Fig. 1) and will be covered by a combination light shield and thermal blanket. In order to minimize the γ-ray background from cosmic-ray interactions in the thermal blanket and light shield, it is essential to minimize their thickness (gm cm^{-2}) and to place these materials as close as possible to the anticoincidence scintillator. The thickness of the combined thermal blanket and light shield is $\sim$ 0.08 g cm^{-2}. This will generate a γ-ray background (> 100 MeV) equivalent to less than 8% of the celestial diffuse flux for 85% of the orbit and less than 3% for 50% of the orbit.

E. Spark Chamber System

The spark chamber system is divided into two sections, separated by the upper scintillator tile array. The upper section, within which the γ-ray is required to convert, consists of 28 spark chamber modules each of active area 81 cm x 81 cm, interleaved with tantalum sheets 0.02 radiation lengths (r.l.) in thickness. The module-to-module spacing is 16.6 mm. The lower section of the spark chamber system, located between the upper and lower scintillator tile arrays, contains six spark chamber modules interleaved with tantalum foils 0.007 r.l. in thickness. Its function is to define the electron-positron trajectories until they intersect the lower tile array and the upper face of the NaI(Tl) crystal. Each spark chamber module contains 992 wires in each of two parallel planes, with the wires in one plane orthogonal to those in the other. The track information is digitized by ferrite cores associated with each grid wire.

Upon receipt of the proper coincidence signal, the spark chambers are pulsed by a group of high voltage switching circuits. The redundant pulser system, including the high voltage converters, interface circuitry and the high voltage switching devices, is housed adjacent to the spark chamber units in pressure-tight containers. Laboratory tests have shown that the high voltage pulser capability easily exceeds the number of pulses required ($\sim 10^8$) over a two year period under reasonable trigger rate assumptions. The high voltage output is programmable by command to allow in-flight shifting of the operating point. The information contained in the approximately 6.6×10^4 cores is read out and compressed to about $(1.0 \text{ to } 1.2) \times 10^3$ bits for a typical event without loss of information.

The selection of the magnetic core spark chamber as the best track imaging device currently available for a high energy γ-ray instrument on GRO was based on a consideration of the following factors: proven feasibility within the constraints of weight, power, and cost; excellent multiple track efficiency with no increase in complexity, power or cost; very high reliability; inherent and long-term track location accuracy; good resolution of close tracks; only two planes of wires to obtain information on two coordinates; freedom from contamination and deterioration over long periods; and long-term stability. The decision was based not only on long experience with these detectors, but also on work with several other types of track imaging systems, including multiwire proportional chambers, magnetostrictive spark chambers, delay line proportional chambers, and proportional drift chambers.

F. Crystal Spectrometer

The function of the NaI(Tℓ) crystal located immediately below the lower tile array is to absorb the energies of the secondary particles from the γ-ray interaction and thereby to indicate the γ-ray energy. This crystal, which measures 76 cm x 76 cm in cross section and 8 r.l. (20 cm) in depth, is too large to prepare, at present, from one crystal ingot. Instead it will be assembled by bonding together, with a clear epoxy, smaller pieces of the ruggedized form of NaI(Tℓ) known as Polyscin I. The bonded crystal is mounted in a sealed container with a thin upper membrane and viewed from below through a shallow light diffusion box by an array of sixteen 12.7 cm photomultiplier tubes. Test measurements of the mechanical properties of Polyscin I have been made and the results show that the expected stress levels in the crystal are well below safe limits for the container design envisaged[3].

The outputs from two groups of 8 photomultiplier tubes are linearly summed and each summed output is fed to one of two identical but independent electronic systems. Each of these pulses is digitized over the dynamic range of 10^3 with a 14-bit linear ADC operating at a clock frequency of 64 MHz. The bit count of 14 is a good match to the energy resolution available from the crystal, and high clock frequency is required by the need to time the crystal pulse to ∿ 15 nsec relative to the MET in order to recognize significant pulse pile-up. Also, hazard flags are recorded that are able to reveal the accidental deposition of energy in the crystal up to ∿ 30 μsec before the event of interest. A parallel mode of operation of the crystal is also provided in which the energy spectrum in the range 0.1 - 20 MeV is monitored with 8-bit resolution in a low energy electronic subsystem for later correlation with other evidence of γ-ray bursts or solar activity.

In flight, the calibration of the crystal spectrometer will be monitored with the aid of a special mode of the event trigger logic. In this mode, signals from the anticoincidence dome will be ignored, the spark chambers will not be pulsed, and crystal pulses will be analyzed only upon receipt of coincidences between corresponding non-peripheral scintillator tiles in each of the tile arrays. This trigger mode will respond to cosmic ray protons, for which the most probable ionization energy loss in the crystal will be $\sim$ 140 MeV.

G. Electronics System

Fig. 2 shows a block diagram of the telescope electronics. The experiment data consist of both primary event data and housekeeping information. Primary event data occurs asynchronously and consists of variable length data blocks which, on average, contain $\sim 10^3$ bits per block. Upon receipt of the MET and after the pulsing of the spark chamber, an event multiplexer interrogates the spark chamber read-out electronics, the crystal data, the digitized time-of-flight, the system clock, and a number of flags that describe the particular event trigger. This information is loaded into a data buffer, which provides for a smoothing of the data transmission rate and makes the experiment dead-time negligibly small for the expected rate of events.

The housekeeping data include secondary scientific data, such as the low energy crystal data, as well as counter and logic rates, command status words, temperatures, pressures and experiment live-time. These data are read out in a fixed format.

H. Mechanical System

An isometric view of the instrument is shown in Fig. 3. The principal structural element, from which the other major sub-assemblies are supported, is the bulkhead pedestal. In addition, the bulkhead pedestal forms the lower surface of the pressure vessel and provides the attachment points to the spacecraft.

I. Instrument Properties

The overall properties of the instrument are summarized below.

TABLE I

Weight	1537 kg (3388 lb)
Size	225 cm (88-in.) x 165 cm (65-in.) max. diameter
Power	98.5 w
Bit Rate	5.0×10^3 s^{-1}
Field-of-View	Average opening angle from experiment axis is 40^o (maximum 45^o)
Commands (Relay)	62
(Data)	8 x 16 bits
Design Lifetime	2 years

III. INSTRUMENT PROPERTIES

A. Introduction

The performance estimates outlined below are based on Monte Carlo and analytic calculations whose essential reliability have been verified by earlier applications to well-calibrated γ-ray telescopes, similar in concept but smaller than the GRO telescope, and to laboratory γ-ray spectrometers. Before launch, the flight instrument will be extensively calibrated in γ-ray beams over a wide range of incident energies and angles in order to obtain the response function that will be used in the analysis of flight data.

B. Angular Resolution

The arrival direction of each γ-ray is estimated from the information in the spark chamber picture. This estimate, defined as the projected r.m.s. error, is 1.6^o at 100 MeV, 0.6^o at 500 MeV and 0.2^o at 2000 MeV. The average angle is 20% smaller and the 3-dimensional r.m.s. angle is 40% larger.

The ability of the instrument to determine the location of a point-source in the sky, or the structure of an extended source, depends on several factors. These include the angular error for each γ-ray, the number of γ-rays detected, the energy spectrum of the detected γ-rays, the energy resolution of the instrument, the intensity of the celestial diffuse γ-ray background, and the uncertainty contributed by the aspect system of the spacecraft. The number of γ-rays detected depends in turn on the strength of the source and the sensitivity of the telescope (see Section IIIC). The design of the GRO telescope takes all these factors into account and the angular resolution achieved approaches the limit imposed by the physics of the conversion process itself. If the spacecraft aspect is known to 2 arcmin, the positions of point-sources will be measured to within 10 arcmin for most regions of the galactic plane, assuming source energy spectra similar to those of known sources. The positions of strong sources, or those well off the galactic plane, may be determined to 5 arcmin.

C. Sensitivity and Field-of-View

The product of the active area (6.6×10^3 cm^2) and the γ-ray detection efficiency is shown versus γ-ray energy and angle in the upper part of Fig. 4. The detection efficiency includes the efficiencies for γ-ray conversion, for triggering, and for γ-ray recognition in the spark chamber picture. The lower part of Fig. 4 shows the effective area integrated over the aperture. The values in Fig. 4 are about 20 times larger than those for SAS-2 and COS-B above 100 MeV and become relatively even larger below 100 MeV since the useful response of the present instrument extends to lower energies. If the Crab pulsar is observed along the telescope axis for 30 days, the detected number of γ-rays above 100 MeV will be ∿ 5400. The sensitivity and angular resolution will allow localized sources 30 - 100 times weaker than the Crab to be

recognized. The wide field-of-view ($\sim 40^{\circ}$ FWHM) will allow several sources to be observed simultaneously, while also including either the galactic plane emission or the diffuse extra-galactic flux. The number of diffuse γ-rays above 100 MeV that can be observed in a six month period will be $\sim 6.6 \times 10^4$.

D. Energy Resolution

The energy resolution provided by an 8 r.l. thick NaI(Tℓ) crystal is easy to measure and to calculate, and is better than 15% FWHM for γ-ray energies less than about 1 GeV. In addition to energy leakage fluctuations from the lower face of the crystal, the effects of which decrease with decreasing γ-ray energy, the realizable energy resolution in the telescope itself is influenced by two other instrumental factors in the range below 1 GeV. These are (1) the presence of $\sim$ 0.6 r.l. of inert material above the crystal, in which the electron-positron pair will deposit a variable amount of energy, and (2) the possibility that one of the secondary particles either is scattered in this inert material and strikes the crystal close to its edge or misses it entirely. In the event analysis, however, partial corrections can be made for both of these effects. The spark chamber reveals the γ-ray conversion point and the subsequent track lengths for the secondary particle pair through the inert material for each event, and a correction can be made for the mean energy lost in this material below the conversion point. For a particle that fails to hit the crystal, an energy estimate can be made by observing its scattering in the upper and lower spark chamber arrays. The influence of both of these effects on the energy resolution have been examined by a Monte Carlo simulation of events in the telescope.

Fig. 5 shows the results obtained when the full aperture of the instrument is illuminated with 120 MeV γ-rays from 6° off the axis. The dotted curve shows the distribution of deposited energy in the crystal for all event triggers.

The dashed curve shows the energy distribution obtained when the mean energy loss in the tantalum plates is added, and the solid curve shows the final result obtained when the energy of any particle missing the crystal, estimated from multiple scattering observations, is also added. The peak sharpens considerably as these corrections are made and the resolution improves from 37 to 17%. The resolution is here defined with respect to the minimum energy window that can be found within which 68% of the events are contained. In this way the asymmetry of the peak profiles is properly reflected. Fig. 6 summarizes the results obtained as a function of γ-ray energy from 20 - 1000 MeV. The correction for energy loss in the plates becomes increasingly important with decreasing γ-ray energy, since the energy loss itself is relatively unchanged. The correction for particle escape disappears at a sufficiently low energy, because of the limited range of the relevant secondary particle. Both corrections are relatively unimportant at energies above 1000 MeV. An even better energy resolution can be obtained for the class of events in which both secondary particles enter the crystal. These results are summarized in Fig. 7. The fraction of triggers which fall into this class increases with increasing γ-ray energy and is approximately 50% at 300 MeV. At energies above 1000 MeV the resolution is expected to degrade slowly to about 25% at 20 GeV due to fluctuations in energy leakage from the lower face of the crystal.

IV. CONCLUSION

The high energy γ-ray telescope described above should be able to extend greatly our knowledge of high energy astrophysics. This will be achieved by defining the structure of the Galaxy with much greater clarity than earlier instruments, by identifying point-sources presently observed but not yet identified, by establishing the nature of the diffuse radiation, and by significantly reducing the threshold for point-source detection. The latter, in addition to producing a much broader knowledge of high energy phenomena in the Galaxy, will open the field of extragalactic γ-ray astronomy, allowing a new view of normal galaxies as well as of active galaxies such as Seyfert galaxies, quasars and BL Lac objects.

ACKNOWLEDGEMENT

The authors wish to acknowledge the contributions of Dr. R. F. Schilling, while at Stanford University, to the early development of this instrument.

REFERENCES

(1) R.W. Ross and J.R. Chesney, Proceedings of the IEEE 1979 Nuclear Science Symposium, Oct. 17-19, 1979, San Francisco, Calif. (following article.)

(2) G. Kettenring, Nucl. Instr. and Meth. 131, 451 (1975).

(3) A systematic test program is now underway, using many more crystal samples cut from known locations in representative crystal forgings, to define the mechanical properties of Polyscin I in detail.

FIGURE CAPTIONS

Fig. 1 A schematic drawing of the telescope.

Fig. 2 A block diagram of the instrument electronics.

Fig. 3 An isometric drawing of the high energy γ-ray telescope.

Fig. 4 Curves showing the sensitivity of the telescope. The solid segments indicate the energy range within which the sensitivity is established from earlier experience with the well-calibrated instruments on SAS-2 and COS-B.

Fig. 5 The energy distribution functions expected for 120 MeV γ-rays from the NaI(Tℓ) crystal alone, and after correction for plate loss and escaping particles.

Fig. 6 The estimated energy resolution, before and after correction for plate loss and escaping particles, for all event triggers.

Fig. 7 The estimated energy resolution, before and after correction for plate loss, for event triggers in which both electron and positron strike the NaI(Tℓ) crystal.

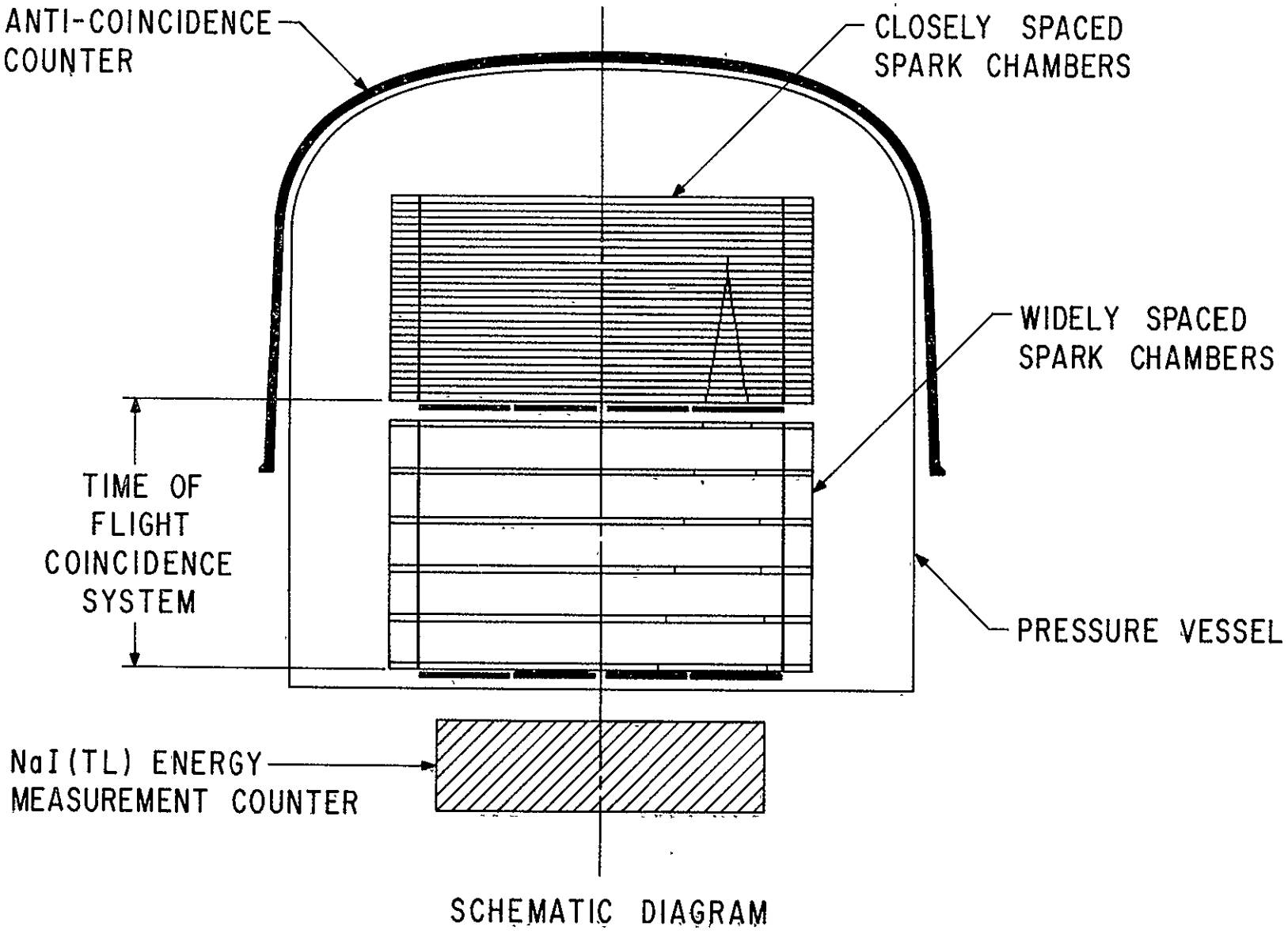
ANTI-COINCIDENCE COUNTER
CLOSELY SPACED SPARK CHAMBERS
WIDELY SPACED SPARK CHAMBERS
TIME OF FLIGHT COINCIDENCE SYSTEM
PRESSURE VESSEL
NaI(TL) ENERGY MEASUREMENT COUNTER
SCHEMATIC DIAGRAM

Fig. 1

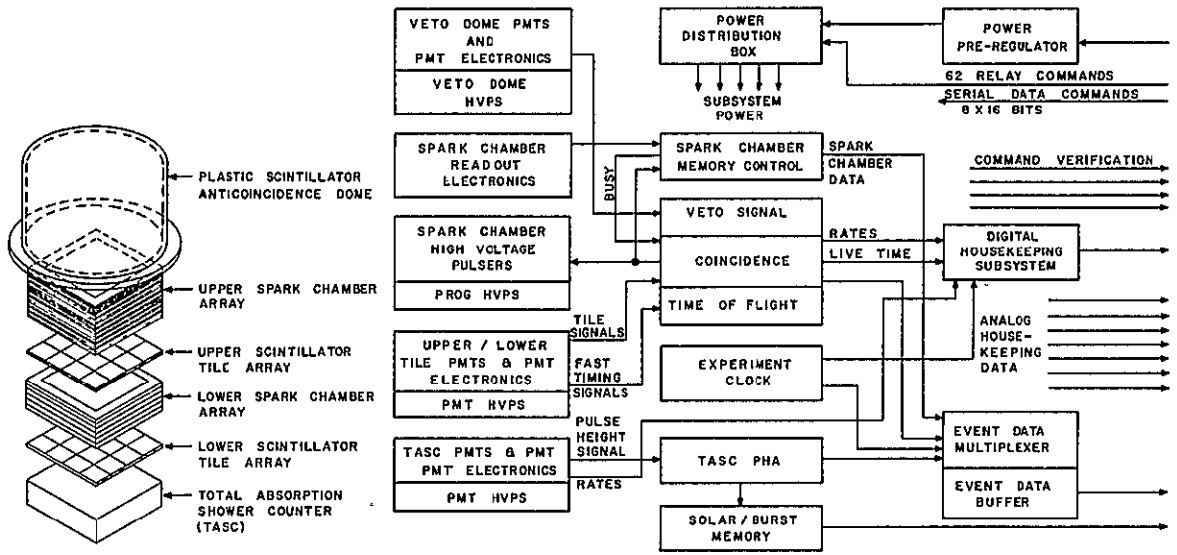

EXPERIMENT BLOCK DIAGRAM

Fig. 2

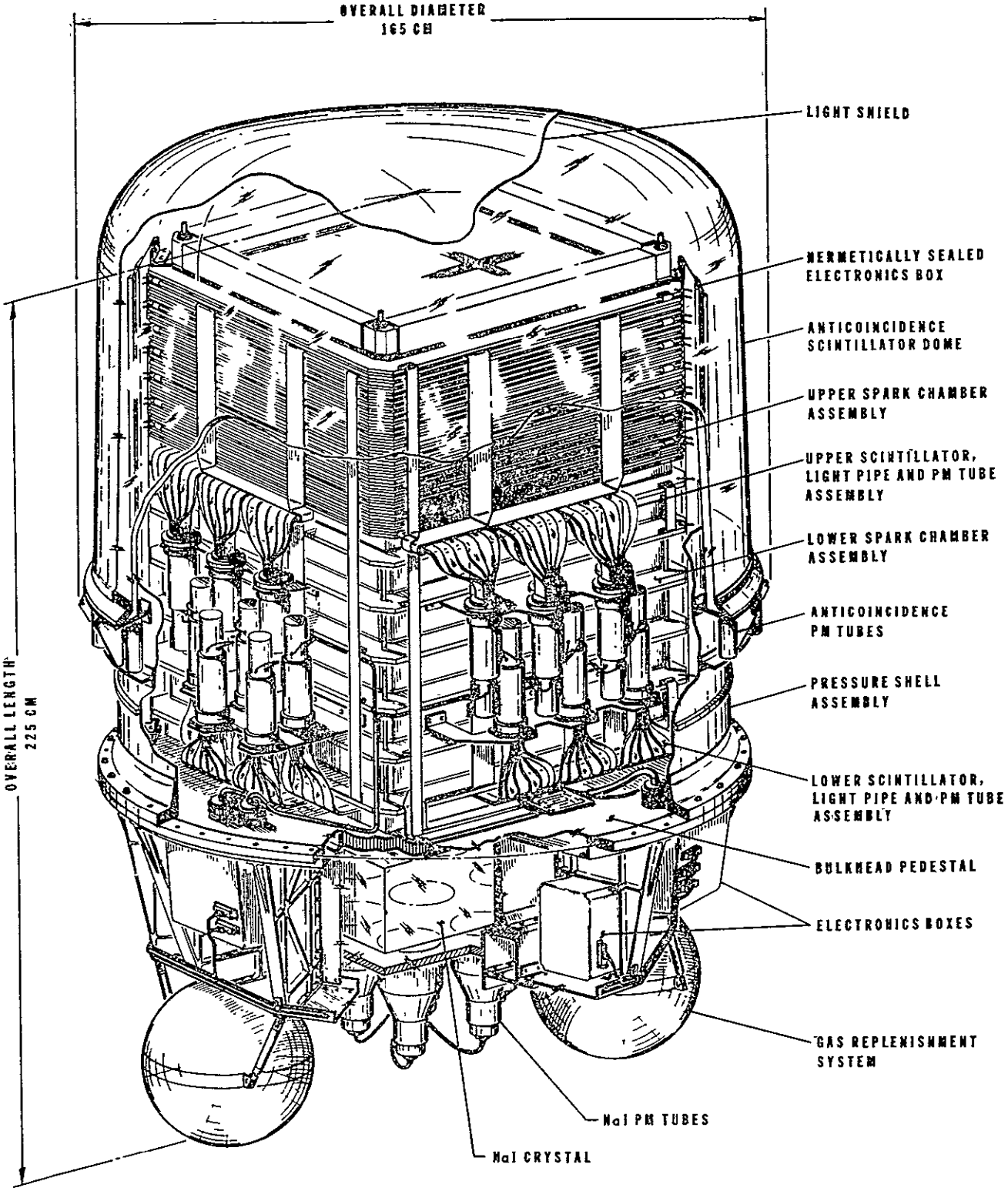
OVERALL DIAMETER
165 CM
OVERALL LENGTH
225 CM
LIGHT SHIELD
HERMETICALLY SEALED
ELECTRONICS BOX
ANTICOINCIDENCE
SCINTILLATOR DOME
UPPER SPARK CHAMBER
ASSEMBLY
UPPER SCINTILLATOR,
LIGHT PIPE AND PM TUBE
ASSEMBLY
LOWER SPARK CHAMBER
ASSEMBLY
ANTICOINCIDENCE
PM TUBES
PRESSURE SHELL
ASSEMBLY
LOWER SCINTILLATOR,
LIGHT PIPE AND PM TUBE
ASSEMBLY
BULKHEAD PEDESTAL
ELECTRONICS BOXES
GAS REPLENISHMENT
SYSTEM
NaI PM TUBES
NaI CRYSTAL

Fig. 3

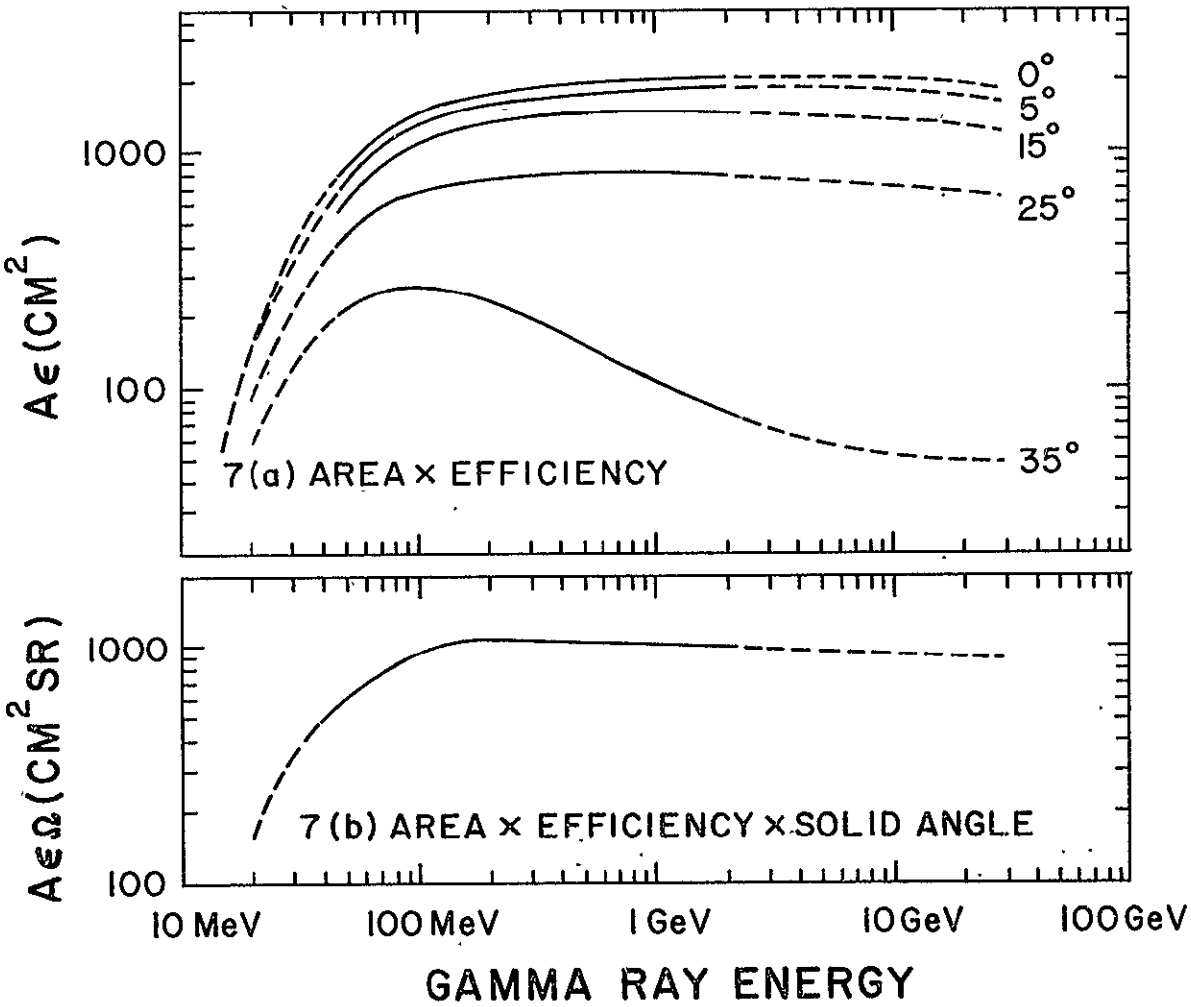
1000
100
Aε (CM²)
0°
5°
15°
25°
35°
7(a) AREA × EFFICIENCY
1000
100
Aεω (CM² SR)
7(b) AREA × EFFICIENCY × SOLID ANGLE
10 MeV
100 MeV
1 GeV
10 GeV
100 GeV
GAMMA RAY ENERGY

Fig. 4

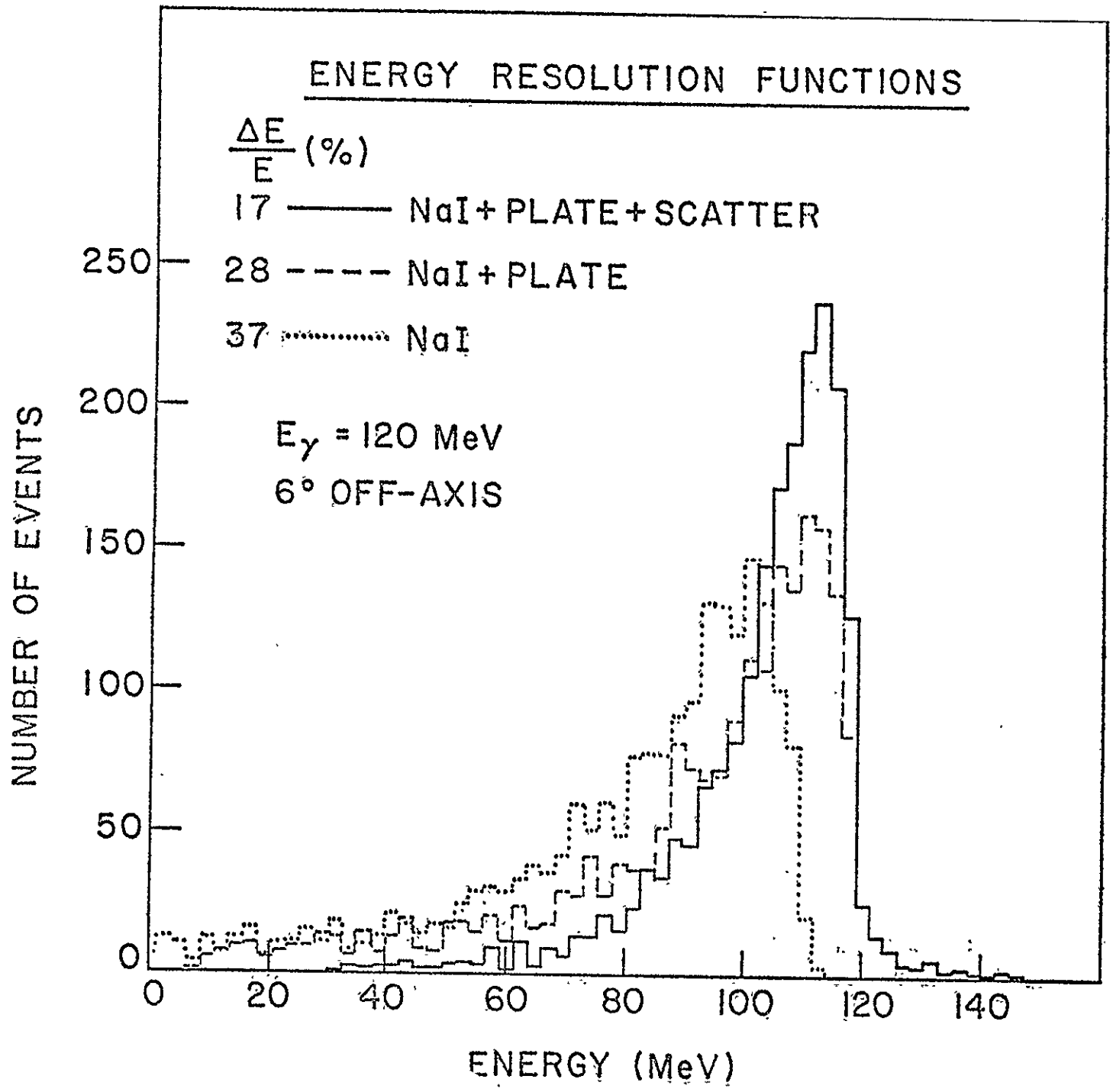
ENERGY RESOLUTION FUNCTIONS
ΔE/E (%)
17 —— NaI+PLATE+SCATTER
28 ---- NaI+PLATE
37 ..... NaI
Eγ = 120 MeV
6° OFF-AXIS
NUMBER OF EVENTS
ENERGY (MeV)
0
50
100
150
200
250
0
20
40
60
80
100
120
140

Fig. 5

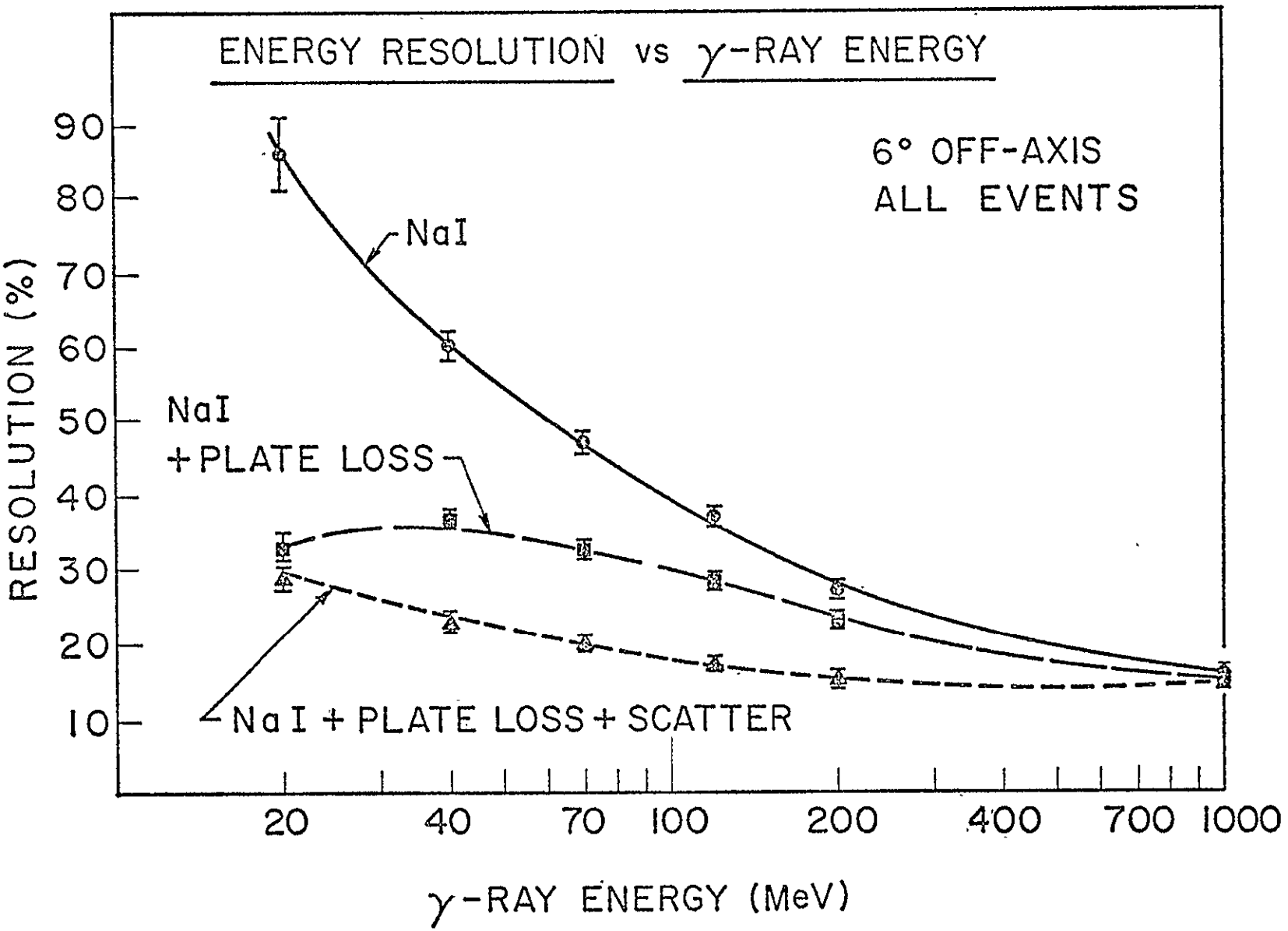
ENERGY RESOLUTION vs γ-RAY ENERGY
6° OFF-AXIS
ALL EVENTS
NaI
NaI
+PLATE LOSS
NaI + PLATE LOSS + SCATTER
RESOLUTION (%)
90
80
70
60
50
40
30
20
10
20
40
70
100
200
400
700
1000
γ-RAY ENERGY (MeV)

Fig. 6

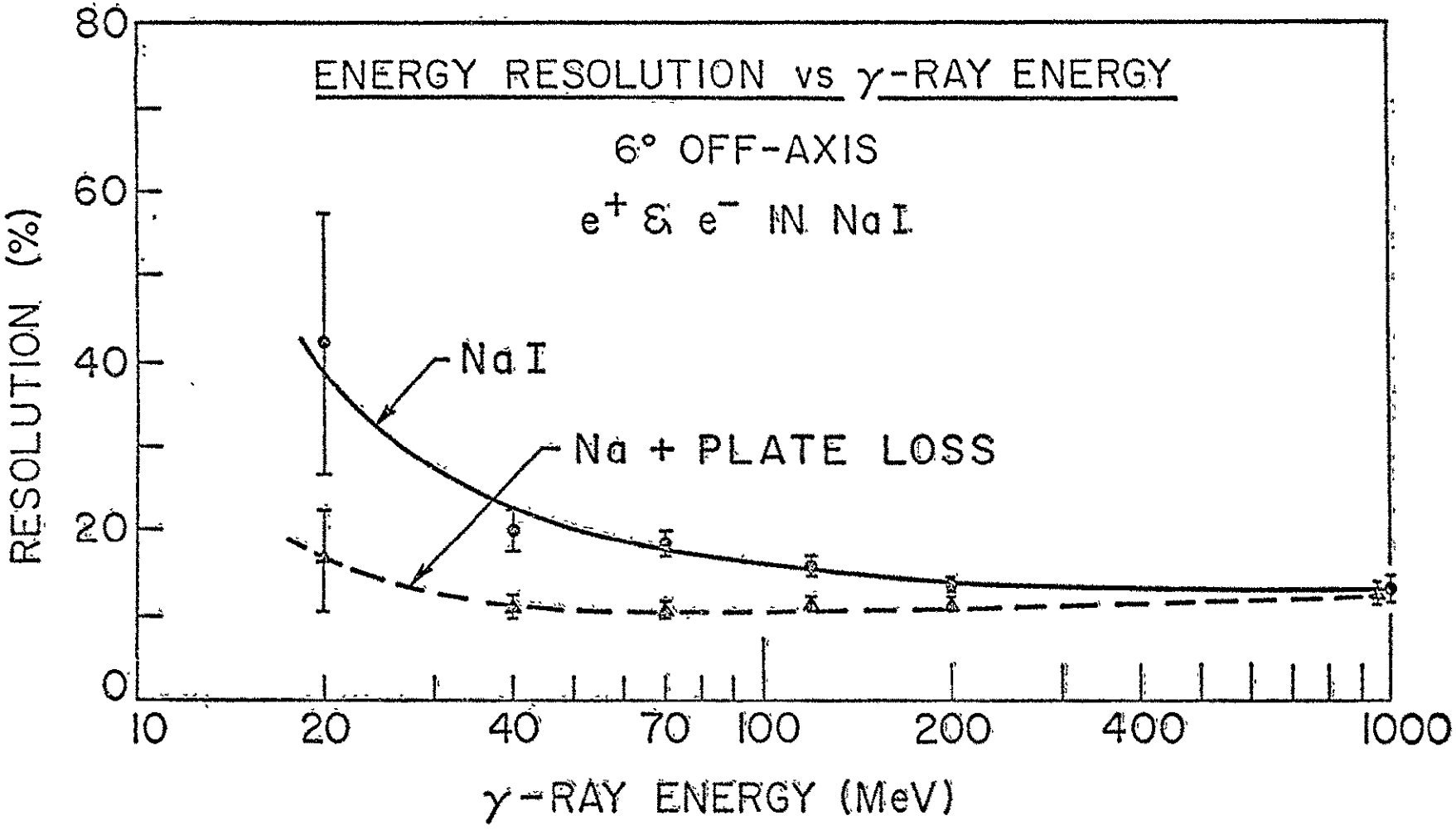
ENERGY RESOLUTION vs γ-RAY ENERGY
6° OFF-AXIS
e+ & e− IN NaI
NaI
Na + PLATE LOSS
RESOLUTION (%)
0
20
40
60
80
10
20
40
70
100
200
400
1000
γ-RAY ENERGY (MeV)

Fig. 7

BIBLIOGRAPHIC DATA SHEET

1. Report No.	2. Government Accession No.	3. Recipient's Catalog No.
TM 80590		

4. Title and Subtitle	5. Report Date
Characteristics of the Telescope for High Energy γ-Ray Astronomy Selected for Definition Studies on the Gamma Ray Observatory	October, 1979
	6. Performing Organization Code 660
7. Author(s) Bertsch, Cruickshank, Ehrmann, Fichtel Hartman, Kniffen, Ross, Thompson	8. Performing Organization Report No. 662
9. Performing Organization Name and Address Laboratory for High Energy Astrophysics NASA/Goddard Space Flight Center Greenbelt, MD 20771	10. Work Unit No.
	11. Contract or Grant No.
	13. Type of Report and Period Covered TM
12. Sponsoring Agency Name and Address NASA/Goddard Space Flight Center Greenbelt, MD 20771	14. Sponsoring Agency Code

15. Supplementary Notes

Presented at IEEE 1979 Science Symposium Oct. 17-19, 1979, San Francisco, Ca.

16. Abstract

The high energy γ-ray selected for definition studies on the Gamma Ray Observatory provides a substantial improvement in observational capability over earlier instruments. It will have about 20 times more sensitivity, cover a much broader energy range, have considerably better energy resolution and provide a significantly improved angular resolution. The design and performance are described.

17. Key Words (Selected by Author(s))	18. Distribution Statement
Gamma rays, high energy Gamma Ray Observatory	

19. Security Classif. (of this report)	20. Security Classif. (of this page)	21. No. of Pages	22. Price*
unclassified	unclassified	24	

*For sale by the National Technical Information Service, Springfield, Virginia 22151.

GSFC 25-44 (10/77)